Synthesis and Characterization of Three Novel Perfluoro-oligothiophenes Ranging in Length from the Trimer to the Pentamer

Reyes Malavé Osuna,[†] Rocío Ponce Ortiz,[†] Mari Carmen Ruiz Delgado,[†] Youichi Sakamoto,[‡] Toshiyasu Suzuki,[‡] Víctor Hernández,[†] and Juan T. López Navarrete*[,†]

Department of Physical Chemistry, University of Málaga, 29071-Málaga, Spain, and Institute for Molecular Science, Myodaiji, Okazaki 444-8585, Japan

Received: July 29, 2005; In Final Form: September 7, 2005

In this Article, we report on the synthesis and full characterization of three perfluorinated oligothiophenes, ranging in length from the trimer to the pentamer (**PF-*n*T**, with $n = 3$, 4, or 5). The differential pulse voltammetry (DPV) analysis of the compounds showed that they can be both oxidized and reduced (i.e., they display a dual or amphoteric electrochemical behavior), with the reduction peaks positively shifted relative to those of the corresponding unsubstituted oligothiophenes. The electrochemically determined energy gaps are in agreement with those measured from the UV−vis−NIR absorption spectra in solution. The conjugational properties have been investigated by means of FT-Raman spectroscopy, both as pure solids and as dilute solutes in CH_2Cl_2, revealing that: (i) π-conjugation does not still reach saturation with chain length for the longest oligomer, and (ii) conformational distortions from a nearly coplanar arrangement of the successive thiophene units upon solution are not too large. DFT and TDDFT quantum chemical calculations have been performed, at the B3LYP/6-31G** level, to assess information about the optimized molecular structure, equilibrium atomic charges distribution, energies and topologies of the frontier molecular orbitals (MO) around the gap, vibrational normal modes associated with the most outstanding Raman scatterings, and vertical one-electron excitations that give rise to the main optical absorptions.

I. Introduction

Oligothiophenes have received great attention over the past 15 years because of their quite relevant optoelectronic properties and potential applications in a variety of devices such as organic-emitting diodes (OLEDs)[1] and field-effect transistors (FETs).[2] Their ability in FETs is particularly attractive, and there have been many efforts toward improving the two important characteristics, on−off ratio and mobility. Recent attempts to improve the FETs include the use of highly purified oligomers,[3] high-temperature film deposition,[4] and single-crystals,[5] leading to better ordering of the molecules in the thin film and therefore improved transistors performance. Different chemical modifications have been proposed as well. The use of alkyl side groups at the end α,ω-positions of the oligothienyl backbone has also been investigated. This strategy has the 2-fold benefit of blocking these positions to further reactions, that is, oxidation and polymerization, and of improving the crystal ordering. High mobility was achieved upon the replacement of the end α,ω-hydrogens of sexithiophene by *n*-hexyl groups.[6] Less success was met instead with methyl,[2e,7] ethyl,[2d] and hexylthio[8] end-capping groups.

On the other hand, organic n-type semiconductors,[9] which are important components for complementary circuits, are few and difficult to develop as compared to p-type ones. One might devise ambipolar FETs using a π-conjugated oligomer that acts as both a p-type and an n-type semiconductor when properly polarized. Oligothiophenes easily form stable radical cations and higher oxidation states at rather low potentials, whereas they are usually quite difficult to reduce and do not form stable anion radicals or dianions. Thus, oligothienyl materials that might be both oxidizable and reducible are quite interesting for FET applications.

Some of us have reported in the recent past that perfluorination of an organic p-type semiconductor is an effective way to prepare an n-type semiconductor.[10] For example, perfluorinated oligo-(*p*-phenylene)s were found to act as efficient n-type semiconductors for the fabrication of the electron-transport layer in OLEDs.[10a]

Whether π-conjugated oligomers showing an amphoteric redox behavior find, for example, FET applications depends on properly developing and understanding their structure, chemistry, and physicochemical properties. In this Article, we report on the synthesis and characterization of three perfluorinated oligothiophenes, ranging in length from the trimer to the pentamer, paying particular attention to their electrochemical and optical properties (see Scheme 1). We also investigate the chain-length dependence of their π-conjugational properties by means of Raman spectroscopy, both as pure solids and as dilute solutes. The whole set of experimental data are interpreted with the help of DFT and TDDFT quantum chemical calculations, at the B3LYP/6-31G** level, regarding the minimum-energy molecular structure, equilibrium atomic charges distribution, topologies and absolute energies of the frontier molecular orbitals (OMs) around the gap, vibrational normal modes associated with the most outstanding Raman features selectively enhanced by the effective π-conjugation, and vertical one-electron excitations giving rise to the main electromagnetic absorption in the visible spectral region.

II. Experimental and Theoretical Details

Fourier transform infrared absorption (FT-IR) spectra were recorded on a Bruker Equinox 55 spectrometer. Compounds

* Corresponding author. E-mail: teodomiro@uma.es.
[†] University of Málaga.
[‡] Institute for Molecular Science.

10.1021/jp054205b CCC: $30.25
Published on Web 10/14/2005

SCHEME 1

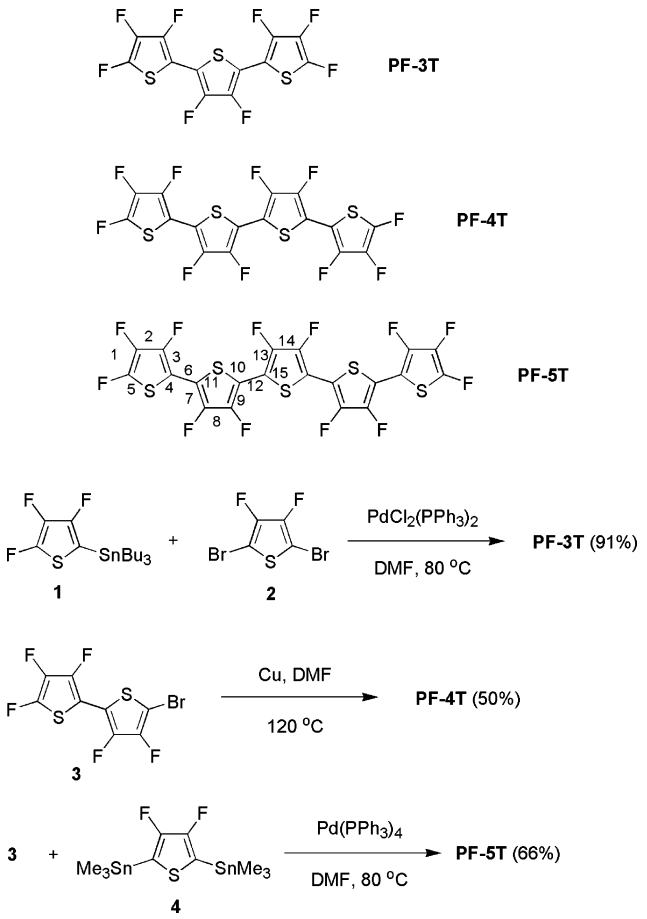

were ground to a powder and pressed in KBr pellets. FT-IR spectra, with a spectral resolution of 2 cm^{-1}, were collected and were the average of 50 scans. Interference from atmospheric water vapor was minimized by purging the instrument with dry argon before starting the data collection. FT-Raman scattering spectra were collected on a Bruker FRA106/S apparatus and a Nd:YAG laser source (λ_{exc} = 1064 nm), in a backscattering configuration. The operating power for the exciting laser radiation was kept to 100 mW in all of the experiments. Samples were analyzed as pure solids in sealed capillaries and dilute CH_2Cl_2 solutions (supplied by Aldrich with analytical grade). Typically, 1000 scans with 2 cm^{-1} spectral resolution were averaged to optimize the signal-to-noise ratio. UV−vis−NIR absorption spectra were recorded on an Agilent 8453 instrument equipped with a diode array for a fast record of the whole electronic spectrum in the 190−1100 nm spectral region.

Differential pulse voltammetry (DPV) was recorded on a BAS-100B/W electrochemical analyzer, by using a three-electrode configuration. All measurements were performed at room temperature under an argon atmosphere in a 0.1 M 1,2-dichlorobenzene solution of $(n\text{-Bu})_4NPF_6$. The concentrations of oligothiophenes ranged from 10^{-4} to 10^{-3} M. A platinum working electrode (1-mm diameter) was polished with 0.05-μm alumina before measurements. A platinum wire was used as the counter electrode. The reference electrode was an Ag/0.01 M $AgNO_3$ electrode filled with 0.1 M $(n\text{-Bu})_4NClO_4$ in CH_3CN. All potentials quoted along the paper are referenced to the ferrocene/ferrocenium couple (Fc/Fc^+) as the internal standard.

Density functional theory (DFT) calculations were carried out by means of the Gaussian 03 program[11] running on an SGI Origin 2000 supercomputer. We used the Becke's three-parameter exchange functional combined with the LYP correlation functional (B3LYP).[12] It has already been shown that the B3LYP functional yields geometries for medium-sized molecules similar to those of MP2 calculations with the same basis sets.[13,14] Moreover, the DFT force fields calculated using the B3LYP functional yield infrared spectra in good agreement with experiments.[15,16] We also made use of the standard 6-31G* basis set.[17] Optimal geometries were determined on isolated entities. All geometrical parameters were allowed to vary independently apart from planarity of the rings. On the resulting ground-state optimized geometries, harmonic vibrational frequencies and infrared and Raman intensities were calculated analytically with the B3LYP functional.

We used the often-practiced adjustment of the theoretical force fields in which calculated harmonic vibrational frequencies are uniformly scaled down by a factor of 0.96 for the 6-31G** calculations, as recommended by Scott and Radom.[14] This scaling procedure is often accurate enough to disentangle serious experimental misassignments. All quoted vibrational frequencies reported along the paper are thus scaled values. The theoretical spectra were obtaining by convoluting the scaled frequencies with Gaussian functions (10 cm^{-1} width at the half-height). The relative heights of the Gaussians were determined from the theoretical Raman scattering activities.

Vertical electronic excitation energies were computed by using the time-dependent DFT (TDDFT) approach.[18,19] The 20 lowest-energy electronic excited states were at least computed for all of the molecules. The computational cost of TDDFT is roughly comparable to that of single-excitation theories based on an HF ground state, such as single-excitation configuration interactions (CIS). Numerical applications reported so far indicate that TDDFT formalism employing current exchange-correlation functionals performs significantly better than HF-based single excitation theories for the low-lying valence excited states of both closed-shell and open-shell molecules.[20,21] TDDFT calculations were carried out using the B3LYP functional and the 6-31G** basis set on the previously optimized molecular geometries obtained at the same level of calculation. Molecular orbital contours were plotted using Molekel 4.3.[22]

Compounds **1**−**3** (see Scheme 1) were synthesized according to a previously reported procedure.[10] Anhydrous THF and DMF were used as received from Kanto Chemicals. Melting points were obtained on a Büchi melting point apparatus B-540. ^1H and ^{19}F NMR spectra were recorded on a JEOL JNM-LA 500 at 500 and 470.4 MHz, respectively. Chemical shifts were reported as δ values (ppm) relative to internal tetramethylsilane (^1H NMR) or hexafluorobenzene (^{19}F NMR). EI mass spectra were obtained on a Shimadzu GCMS-QP5050A at 70 eV. Analytical TLCs were performed on commercial Merck plates coated with silica gel 60 F_{254}. Flash chromatographic separations were carried out on Fuji Silysia FL60D.

3,4,5,3′,4′,3″,4″,5″-Octafluoro-[2,2′;5′,2″]terthiophene (PF-3T). A mixture of **1** (4.10 g, 9.60 mmol), **2** (1.12 g, 4.03 mmol), and $PdCl_2(PPh_3)_2$ (141 mg, 0.201 mmol) in dry DMF (10 mL) was stirred at 80 °C under argon for 3 h. The reaction mixture was allowed to cool to room temperature, poured into aqueous KF solution, and stirred at room temperature for 3 h. The resulting suspension was diluted with CH_2Cl_2 and filtered to remove polymeric tributyltin fluoride. The organic phase was separated, and the aqueous phase was extracted with CH_2Cl_2. The combined organic phase was washed with brine, dried with $MgSO_4$, and concentrated. The residue was chromatographed on silica gel (4:1 *n*-hexane/CH_2Cl_2) to give **PF-3T** (1.44 g,

91%). An analytical sample was prepared by train sublimation at 100 °C under a flow of 1 atm argon: mp 91−92 °C; ^{19}F NMR ($CDCl_3$) δ 31.8 (t, J = 11.7 Hz, 2F), 27.8 (s, 2F), 15.2 (d, J = 11.7 Hz, 2F), 7.7 (d, J = 11.7 Hz, 2F); MS m/z 392, 393, 394, 395 (M^+, 100, 15.1, 14.2, 2.3). Anal. Calcd for $C_{12}F_8S_3$: C, 36.74; S, 24.52. Found: C, 36.95; S, 25.52.

3,4,5,3′,4′,3″,4″,3‴,4‴,5‴-Decafluoro-[2,2′;5′,2″;5″,2‴]-quaterthiophene (PF-4T). A mixture of **3** (1.34 g, 4.00 mmol) and copper bronze (305 mg, 4.80 mmol) in dry DMF (20 mL) was stirred at 120 °C under argon for 4 h. The reaction mixture was allowed to cool to room temperature, then poured into 1 M HCl, and filtered. The resulting yellow solid was washed with *n*-hexane and purified by sublimation in vacuo at 180 °C to afford **PF-4T** (510 mg, 50%): mp 177−178 °C; ^{19}F NMR ($CDCl_3$) δ 32.1 (dt, J = 11.8, 5.5 Hz, 2F), 29.2 (d, J = 11.8 Hz, 2F), 27.8−27.7 (m, 2F), 15.4 (dd, J = 11.8, 7.1 Hz, 2F), 7.8 (d, J = 11.8 Hz, 2F); MS m/z 510, 511, 512, 513, 514 (M^+, 100, 21.6, 19.3, 3.7, 1.7). Anal. Calcd for $C_{16}F_{10}S_4$: C, 37.65; S, 25.13. Found: C, 37.62; S, 26.24.

3,4-Difluoro-2,5-bis-trimethylstannanyl-thiophene (4). To a solution of 2,5-dibromo-3,4-difluoro-thiophene[1] (2.78 g, 10.0 mmol) in THF (40 mL) was added *n*-BuLi in hexane (8.5 mL, 20.9 mmol) at −80 °C under argon, and the mixture was stirred at −80 °C for 30 min. The Me_3SnCl (4.18 g, 21.0 mmol) solution in THF (21 mL) was added dropwise, and the resulting solution was stirred at −80 °C for 1 h. The reaction mixture was allowed to warm to room temperature and poured into H_2O. The organic phase was separated, and the aqueous phase was extracted with ether. The combined organic phase was washed with brine and dried with $MgSO_4$. Removal of the solvent afforded **4** (3.52 g, 79%). An analytical sample was purified by recrystallization from *n*-hexane to give colorless crystals: mp 88−89 °C; ^{19}F NMR ($CDCl_3$) δ 29.3 (s, 2F); ^{1}H NMR ($CDCl_3$) δ 0.39 (s, 18H); MS m/z 427, 428, 429, 430, 431, 432, 433, 434, 435 ($M^+ - CH_3$, 37.7, 19.7, 80.9, 43.3, 100, 33.2, 58.9, 14.1, 18.7). Anal. Calcd for $C_{10}H_{18}F_2SSn_2$: C, 26.95; H, 4.07; S, 7.19. Found: C, 27.00; H, 4.30; S, 7.36.

3,4,5,3′,4′,3″,4″,3‴,4‴,3⁗,4⁗,5⁗-Dodecafluoro-[2,2′;5′,2″;5″,2‴;5‴,2⁗]quinquethiophene (PF-5T). A mixture of **3** (1.01 g, 3.01 mmol), **4** (669 mg, 1.50 mmol), and $Pd(PPh_3)_4$ (173 mg, 0.150 mmol) in dry DMF (20 mL) was stirred at 80 °C under argon for 5 h. The reaction mixture was cooled to room temperature, poured into H_2O, and extracted with CH_2Cl_2. The combined organic phase was washed with brine, dried with $MgSO_4$, and concentrated. The residue was chromatographed on silica gel (4:1 *n*-hexane/CH_2Cl_2) to give **PF-5T** (626 mg, 66%). An analytical sample was prepared by train sublimation at 220 °C under a flow of 1 atm argon: mp 220−221 °C; ^{19}F NMR ($CDCl_3$) δ 32.2−32.1 (m, 2F), 29.5 (d, J = 11.7 Hz, 2F), 29.2 (s, 2F), 27.8−27.7 (m, 2F), 15.5−15.4 (m, 2F), 7.8 (d, J = 11.7 Hz, 2F); MS m/z 628, 629, 630, 631, 632 (M^+, 100, 28.6, 22.0, 5.8, 2.4). Anal. Calcd for $C_{20}F_{12}S_5$: C, 38.22; S, 25.51. Found: C, 37.93; S, 26.90.

III. Results and Discussion

A. UV−Vis Absorption Data. The chemical structures and abbreviate notation of the three perfluorinated oligothiophenes studied in this Article are depicted in Scheme 1, and their normalized electromagnetic absorption spectra are displayed in Figure 1. The chromophores display a strong and broad absorption in the visible spectral region, whose maximum progressively shifts to lower energies as the oligomeric chain grows longer (344 nm in **PF-3T**, 378 nm in **PF-4T**, 401 nm in **PF-5T**). The shape and position of the UV−vis spectral features were found to be concentration-independent in the range examined, suggesting that oligomers are not in an aggregated phase.

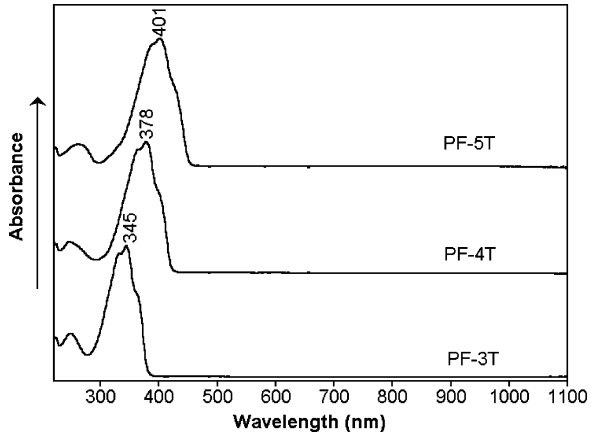

Figure 1. Normalized visible absorption spectra of the **PF-*n*T** (n = 3−5) oligomers in CH_2Cl_2 solution.

TABLE 1: Optimized B3LYP/6-31G Values (in Å) for Selected Skeletal Bond Lengths along the Whole Set of PF-*n*T Oligomers (See Number Bonds in Scheme 1)**

bond	PF-3T	PF-4T	PF-5T
1	1.361	1.361	1.361
2	1.423	1.423	1.423
3	1.372	1.372	1.372
4	1.771	1.772	1.772
5	1.744	1.744	1.744
6	1.439	1.439	1.438
7	1.374	1.374	1.375
8	1.412	1.411	1.411
9		1.375	1.376
10	1.762	1.763	1.764
11		1.761	1.761
12		1.436	1.436
13			1.376
14			1.410
15			1.763

For all of the oligomers, the strongest absorption band near 400 nm displays a well-resolved vibronic structure at room temperature. This observation suggests that there exists a high degree of intramolecular conformational order in solution (i.e., more specifically a large correspondence between the ground and excited state's molecular geometries), which should result in a nearly flat or fully coplanar arrangement of the successive thiophene units, and hence in a high degree of π-electron delocalization.

B. Optimized Geometries and Theoretical Electronic Transitions. To gain a deeper insight into the chain-length dependence of the molecular structure and equilibrium charge distribution of these perfluorinated oligothiophenes, we have performed geometry optimizations, within the framework of the density functional theory, for the whole set of oligomers by using ab initio B3LYP/6-31G** model chemistry. (Table 1 summarizes the optimized distances of selected skeletal bonds for the three **PF-*n*T** oligomers.) Although not reported in full detail, the optimized geometries reveal that (i) the various thienyl units of a given oligomer display similar C_α═C_β and C_β−C_β bond lengths, except for the outermost C_α═C_β bonds of each chromophore, which are the shortest C═C double bonds of the whole π-conjugated path, (ii) the C_α−S and the inter-ring C_α−$C_{\alpha'}$ bonds become slightly shorter and longer, respectively, in going from the center of the oligomer toward its ends, and (iii) the C−F bonds attached either to the α- or to the outermost

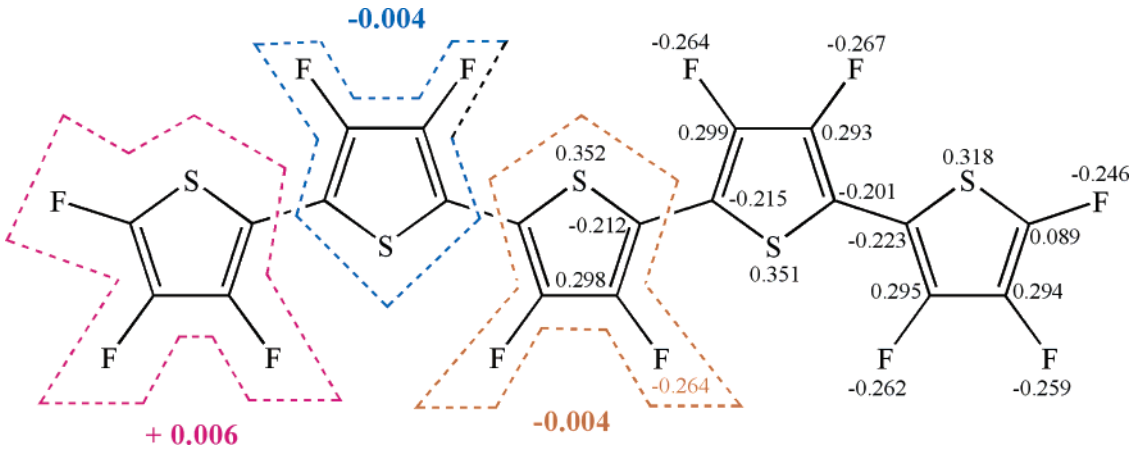

Figure 2. Overall summation (in *e*) of the DFT//B3LYP/6-31G** Mülliken atomic charges on different molecular domains of **PF-5T**, taken as the prototypical example for the other **PF-*n*T** oligomers.

TABLE 2: TDDFT//B3LYP/6-31G Vertical One-Electron Excitations Related to the Strongest Visible Absorption of Each PF-*n*T Oligomer in $CHCl_3$[a]**

oligomer	ΔE_{exp} (eV)	$\Delta E_{B3LYP/6-31G^{**}}$ (eV)	ΔE_{H-L} (eV)	description
PF-3T	3.60 (3.49)	3.34 ($f = 0.88$)	3.48	HOMO → LUMO
PF-4T	3.28 (3.18)	2.92 ($f = 1.32$)	3.08	HOMO → LUMO
PF-5T	3.08 (3.02)	2.65 ($f = 1.74$)	2.84	HOMO → LUMO

[a] The ΔE_{exp} values within parentheses refer to the corresponding unsubstituted oligothiophenes.

β-positions of the end thienyl rings are predicted to be sizably shorter (i.e., 1.329 and 1.335 Å, respectively) than those linked to the inner units (i.e., 1.343 Å). Anyway, DFT model chemistry foresees almost the same geometry for the successive thienyl units from one oligomer to another, so that the molecular parameters are expected to change little upon chain-lengthening (i.e., this theoretical result must be related to the presence of many, highly electronegative, peripheral fluorine atoms surrounding the alternating sequence of C=C/C−C conjugated bonds).

The mean single−double CC bond-length alternation (BLA) parameter noticeably varies from 0.057 to 0.038−0.034 Å in going from the ends toward the center of the oligomer. These BLA values, related to the difference between the average lengths of single and double conjugated CC bonds, can be compared to those computed for other homologous series of oligothiophenes end-capped by different types of electroactive groups.[23] In this regard, the B3LYP/6-31G** BLA parameter for the end rings of **PF-4T** (0.057 Å) is significantly higher than those obtained, at the same level of calculation, for (i) an α,ω-dicyano end-capped quaterthiophene (0.030 Å), (ii) an α,ω-bis(phenyl) end-capped quaterthiophene (0.035 Å), and (iii) an α,ω-dimethyl end-capped quaterthiophene (0.049 Å).[23] Looking at the details, we observe that the C_α=C_β bonds of **PF-4T** are sizably shorter than their counterparts in the other three quaterthienyl systems (i.e., this is particularly the case for the outermost double bond of both end rings), whereas the opposite occurs regarding the C_β−C_β bonds, so that now the longest distances are found for **PF-4T**.

Figure 2 reports the overall summation of the Mülliken atomic charges on each thienyl unit of **PF-5T** as a prototypical case. Calculations indicate that the end rings are slightly charged positively, while all of the inner units are charged negatively. The C_β−F bonds are highly polarized, so that the Mülliken charges on the carbon and fluorine atoms, averaging the values for the various C_β−F bonds, amount to 0.296*e* and −0.263*e*, respectively. We also observe that the charges on the outermost C_α and its nearest sulfur atom greatly vary with respect to their counterparts in the inner rings. In this regard, the values for **PF-5T** are 0.089*e* and 0.318*e* for the outermost C_α and S atoms, respectively, as compared to −0.212*e* and 0.352*e* for the central thiophene.

To provide insight into the UV−vis spectra of the chromophores, TDDFT calculations at the B3LYP/6-31G** level have been performed for all of the oligomers. Transition energies, oscillator strengths, and highest occupied molecular orbital (HOMO)−lowest unoccupied molecular orbital (LUMO) gaps are listed in Table 2 along with the description of the experimental absorptions in terms of the main one-electron vertical excitations. Figure 3 sketches a diagram with the energies of the molecular orbitals around the gap within the series of compounds, whereas Figure 4 shows the topologies of the frontier molecular orbital of **PF-4T**.

As reported in Table 2, the predictions of the TDDFT calculations are in good agreement with the experimental data, and deviations between the measured and calculated excitation energies for the various electronic absorption bands recorded in the visible region (not shown) do not surpass 0.1−0.3 eV. As expected, the strongest absorption at around 400 nm is predominantly built up from the HOMO → LUMO excitation. Figure 4 shows that both frontier orbitals spread over the whole π-conjugated path. As for the HOMO, the C=C bonds are π-bonding and have an alternating phase with respect to their adjacent C=C bonds, whereas for the LUMO, the C=C bonds are π-antibonding and have the same phase as their nearest neighbors. The fluorine atoms are also predicted to slightly contribute to both the HOMO and the LUMO orbitals.

From the schematic diagrams comparing the B3LYP/6-31G** energy levels around the band gap region for both the set of **PF-*n*T** oligomers and their unsubstituted counterparts (Figure 3), we learn that perfluorination of the oligothienyl backbone causes an overall stabilization, by ∼0.5 eV, of both the doubly occupied (i.e., HOMO, HOMO−1, and so on) and the empty (i.e., LUMO, LUMO+1, and so on) frontier orbitals, so that the HOMO−LUMO gaps of these **PF-*n*T** oligomers are theoretically predicted to amount nearly to the same values, within ∼0.05 eV, of those showed by the unsubstituted

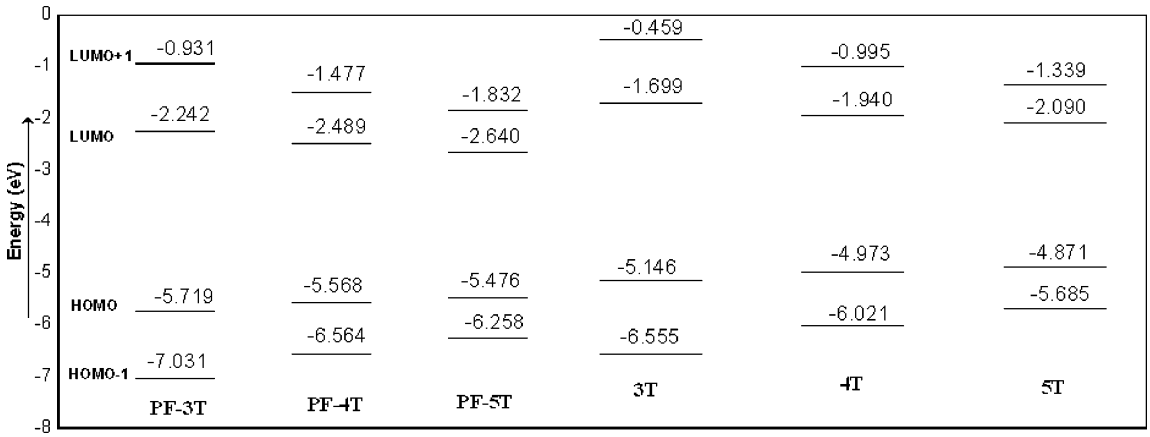

Figure 3. Comparison between the DFT//B3LYP/6-31G** energy levels around the band gap region for the whole set of **PF-*n*T** oligomers and their unsubstituted oligothienyl counterparts.

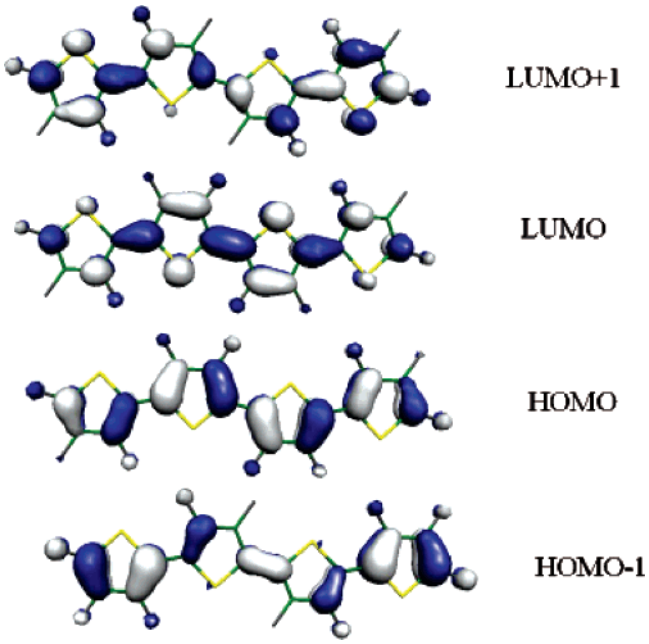

Figure 4. DFT//B3LYP/6-31G** electronic density contours (0.03 e/bohr^3) for the frontier molecular orbitals of **PF-4T**.

oligothiophenes of the same length, in agreement with the great resemblance between the UV−vis absorption spectra of these two kinds of π-conjugated oligomers.

It is worth mentioning that the energy of the vertical electronic transition from a doubly occupied MO to a vacant MO is predicted to be smaller than their energy gap, which might be ascribed to the reduced interelectronic interaction upon the single one-electron excitation (i.e., the interaction can be conceptually interpreted in a simply way as the balance between Coulomb and exchange terms, and expectedly it should decrease progressively with the increasing size of the π-conjugated system). Indeed, the HOMO−LUMO energy gaps for the whole set of **PF-*n*T** oligomers (ΔE_{H-L} in Table 2) are found to be always somewhat higher than the predicted energies for the corresponding HOMO → LUMO one-electron vertical excitations. The fact that the difference between the corresponding ΔE_{H-L} and $\Delta E_{B3LYP/6-31G^{**}}$ values shows an almost negligible dependence on the molecular size (it ranges from 0.14 eV for **PF-3T** to 0.19 eV for **PF-5T**) indicates that the continuous red-shift of the $\pi \rightarrow \pi^*$ visible absorption band with increasing number of units in the chain is mostly caused by the progressive narrowing of the HOMO−LUMO gap, rather than to a distinct interplay of the interelectronic interaction terms (i.e., Coulomb and exchange) in the overall energetic balance from one oligomer to another.

We would like to stress the situation outlined in the preceding paragraphs. First, quite often considered as a direct measure of the effectiveness of the π-conjugation, UV−vis absorption spectra are not unambiguous for this purpose. It is rather usual, when studying a homologous set of α-linked π-conjugated heteroaromatic oligomers, that the optical properties reach saturation for even quite short chain lengths, whereas the orbital energies are theoretically computed to still change sizably for longer oligomers. The Coulomb and exchange integrals are expected to decrease with increasing molecular size (their trend of variation is in line with the assumption that for longer systems the repulsion between charges of the same sign decreases). However, the narrowing of the HOMO−LUMO gap with an increasing number of units in the π-conjugated path is usually larger (i.e., in our case of 0.64 eV from **PF-3T** to **PF-5T**), so that the Coulomb and exchange terms play a minor or secondary role in determining the energy of the singlet excited-state involved in the HOMO → LUMO excitation. As a conclusion of general validity, it is desirable that the analysis of experimental UV−vis data would not be merely based on spectroscopic intuition but helped by some sort of accurate quantum chemical calculations about the energies and topologies of the molecular orbitals, paying attention also to the usual multiconfigurational character of the different electromagnetic absorptions of a given chromophore.

Figure 5 compares the B3LYP/6-31G** absolute energies of the frontier OMs of **PF-3T** to those computed, at the same level of theory, for two other model systems: (i) a terthiophene with its α,ω-positions end-capped by fluorine atoms and (ii) a fully β-fluorinated terthiophene. The α,ω-encapsulation of the oligothienyl backbone with two F atoms leads to a slight stabilization of the doubly occupied and empty frontier OMs, in any case by less than 0.1 eV, with respect to the corresponding energy levels of unsubstituted terthiophene, whereas the frontier OMs for the second model system are much closer in energy to those of **PF-3T**. It follows that the electrochemical and optical properties of these **PF-*n*T** oligomers are mainly determined by the attachment of many peripheral fluorine atoms to the various β-positions of the oligothienyl backbone, rather than to the replacement of the outside α,ω-hydrogens by highly electronegative F atoms. In this regard, we believe it should be interesting to afford the synthesis of a fully β-fluorinated ter- or quaterthiophene with its end α,ω-positions adequately protected, for instance, with triisopropylsilyl groups (i.e., both

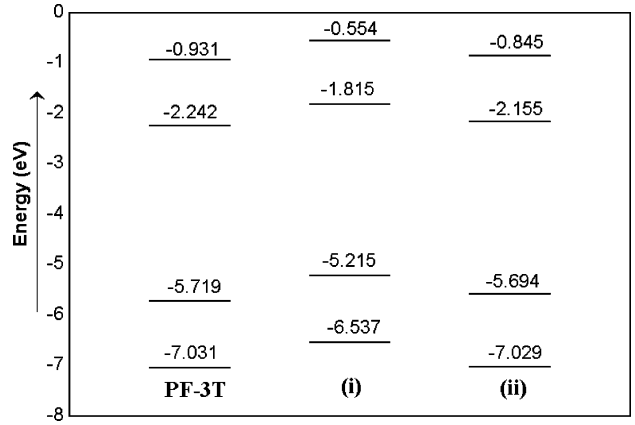

Figure 5. Comparison between the DFT//B3LYP/6-31G** energy levels around the band gap for **PF-3T** and the two other theoretical models: (i) an α,ω-bisfluor end-capped terthiophene and (ii) a fully β-fluorinated terthiophene.

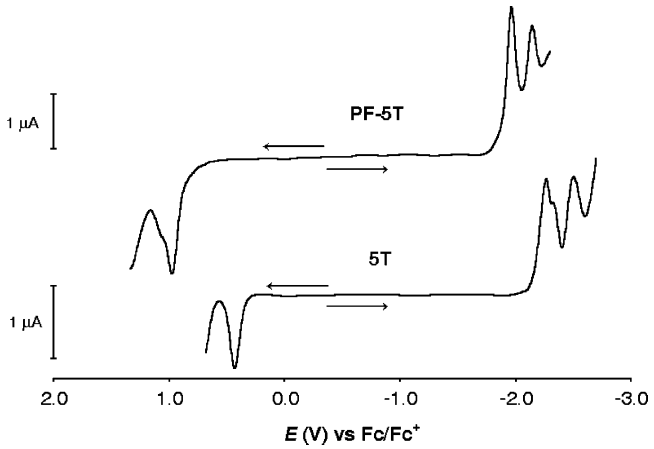

Figure 6. Comparison between the differential pulse voltammograms of **PF-5T** and **5T**.

TIPS groups should be smoothly removed upon treatment with TFA or tetrabutylammonium fluoride, TBAF),[24] with a 2-fold purpose of (i) enhancing solubility of the oligomer in common organic solvents, and (ii) allowing, after protodesilylation, for its further electrochemical polymerization to obtain a fully β-fluorinated polythiophene with, expectedly, a band gap similar to that of polythiophene and an amphoteric redox behavior.

C. Electrochemical Data. The differential pulse voltammogram of each oligomer (see Figure 6) shows a reduction peak as well as an oxidation peak at the potentials summarized in Table 3. As expected, the redox potentials of these perfluorinated oligothiophenes shift positively relative to the corresponding unsubstituted oligothiophenes. The potential differences between the first reduction and oxidation peaks are thus 3.42 V for **PF-3T**, 3.14 V for **PF-4T**, and 2.93 V for **PF-5T**. This result fully agrees with a bathochromic shift of the absorption spectra in passing from **PF-3T** to **PF-5T**.

The electrochemical potentials for the first reduction processes (E^{red} in Table 3) continuously shift to less negative values on increasing number of units in the π-conjugated chain. Assuming that the injected electrons are accommodated into the empty LUMO, Koopman's theorem enables us to relate the absolute LUMO energies with the electrochemical potentials. Because the absolute energy of the HOMO of ferrocene is theoretically estimated to be −4.800 eV (DFT//B3LYP/6-31G**) with respect to the vacuum level and given that the Fc/Fc^+ couple is 0.000 V in the differential pulse voltammetry measurements, it is then possible to quantitatively afford some theory/experiment correlations. DFT model chemistry nicely accounts for the trend of variation of the reduction potentials on increasing chain length; for instance, the E^{red} values for **PF-3T**, **PF-4T**, and **PF-5T** are measured, respectively, at −2.29, −2.11, and −1.96 V, which satisfactorily compare to the calculated −2.56, −2.31, and −2.16 eV values (the latter data are obtained as the difference between the DFT//B3LYP/6-31G** energy of the HOMO of ferrocene and that of the LUMO of each oligomer).

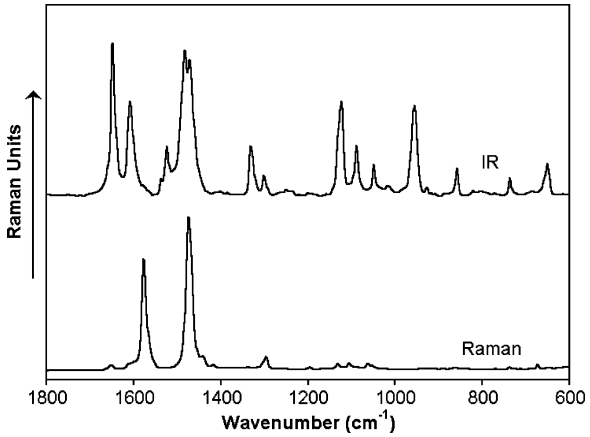

Figure 7. Comparison between the experimental FT-IR and FT-Raman spectra of **PF-3T** in the 2400−600 cm^{-1} spectral range.

TABLE 3: Redox Potentials for the PF-*n*T and *n*T Oligomers Determined by Differential Pulse Voltammetry[a]

oligomer	E^{ox} (V)	E^{red} (V)	ΔE (V)
PF-3T	1.13	−2.29	3.42
PF-4T	1.03	−2.11	3.14
PF-5T	0.97	−1.96	2.93
3T	0.62	−2.60	3.22
4T	0.50	−2.39	2.89
5T	0.44	−2.33	2.77

[a] Voltage values are given against the Fc/Fc^+ couple. Experimental conditions: room temperature; scan rate, 20 mV/s; 0.1 M $(n\text{-}Bu)_4PF_6$ in 1,2-dichlorobenzene; working electrode, Pt disk (1-mm diameter); counter electrode, Pt wire; reference electrode, Ag/0.01 M $AgNO_3$ and 0.1 M $(n\text{-}Bu)_4NClO_4$ in CH_3CN.

The scenario is, however, the opposite for the anodic features, which are shifted to higher energies in passing from the unsubstituted oligothiophenes to their perfluorinated counterparts (see Table 3); this phenomenon is related to the stabilization of the HOMO by ∼0.58 eV from the former to the latter family of compounds. In addition, along the **PF-*n*T** series, the first oxidation potentials are also found to shift to lower values upon chain-lengthening, which again is in accordance with the predictions of the DFT//B3LYP/6-31G** calculations. In this regard, the trend of variation of the E^{ox} values with the chain length is 1.13 versus 0.92 eV for **PF-3T**, 1.03 versus 0.77 eV for **PF-4T**, and 0.97 versus 0.68 eV for **PF-5T** (i.e., the second reported value in each case refers to the difference between the absolute HOMO energies of ferrocene and the perfluoroligothiophene).

D. Experimental and Theoretical Vibrational Spectra. Figure 7 compares the Fourier transform IR (FT-IR) and FT-Raman spectral profiles of **PF-3T**, as the prototypical example for the other oligomers, whereas Figure 8 illustrates the selective enhancement of the skeletal Raman-active vibrations collected for **PF-4T** between 1500 and 1100 cm^{-1}, and Figure 9 depicts the B3LYP/6-31G** vibrational eigenvectors associated with the most outstanding IR and Raman features of **PF-5T**. Finally, Figure 10 compares the Raman scattering profiles recorded for

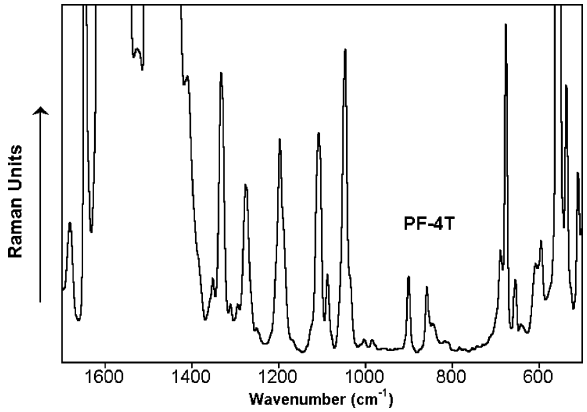

Figure 8. Enlarged profile of the solid-state FT-Raman spectrum of **PF-4T** showing the selective enhancement of particular skeletal ν(CC) stretching vibrations between 1500 and 1100 cm^{-1} with respect to the many Raman scatterings recorded below 1000 cm^{-1}.

the three **PF-*n*T** oligomers in the form of both pure solid samples as well as dilute solutes in CH_2Cl_2.

From the discovery of the electrically conducting polymers, vis−NIR electronic absorption and infrared and Raman vibrational spectroscopies have been widely used to characterize many different types of π-conjugated systems (oligomers and polymers), and among them Raman spectroscopy has been shown to be of great help in (i) analyzing the effectiveness of the π-conjugation along a homologous series of oligomers,[25−27] (ii) characterizing different types of conjugational defects induced by either chemical doping or photoexcitation,[28] and (iii) estimating the degree of intramolecular charge transfer in push−pull π-conjugated chromophores.[29,30]

The observation of rather a few and overwhelmingly strong Raman scatterings, even for systems having complex chemical structures,[27f,28f] was definitively accounted for over 20 years ago by Zerbi and co-workers through the development of the nowadays well-accepted Effective Conjugation Coordinate (ECC) theory, which implicitly postulates the existence of a unique collective C═C/C−C stretching mode strongly involved in the electron−phonon coupling mechanism, which characterizes these one-dimensional π-conjugated chains.[31] In heteroaromatic polyconjugated systems, the so-termed collective ECC coordinate has the analytic form of a linear combination of ring C═C/C−C stretchings, which points in the direction from a benzenoid structure (usually that of the ground electronic state) to a quinonoid one (that corresponding to the electronically excited state). The ECC formalism states that the totally symmetric C═C/C−C stretching modes entering in the lattice dynamics of the ECC vibrational coordinate (those that give rise to the few and selectively enhanced Raman features) should undergo large dispersions both in peak position and in intensity on increasing conjugation length along a given set of neutral oligomers. Thus, changes in Raman frequencies and relative intensities with increasing chain length are particularly useful in evaluating the mean conjugation length for a given family of π-conjugated compounds. Furthermore, upon chemical or electrochemical oxidation/reduction of these π-conjugated heteroaromatic systems, various types of quinonoid-like charged defects are created.[32] The subsequent quinoidization of the π-conjugated backbone gives rise to a further red-shift of the strongest Raman lines (due to the progressive softening of the conjugated C═C bonds), which is a marker of the type of charged defects created upon oxidation or reduction.[25−28]

Figure 7 shows again for these perfluorinated oligothiophenes the usual simplicity of their Raman spectra as compared to the IR absorption profiles; the former display only two main features (i.e., near 1570 and 1470 cm^{-1}) associated with skeletal ν(C═C) stretching modes, whereas for the latter a number of strong IR absorptions are still recorded below 1100 cm^{-1} (i.e., some of them, as the medium-strong IR feature near 960 cm^{-1}, being due to in-plane δ_{ring} bending modes, fully decoupled from the π-electron degree of freedom, but which acquire however a strong IR-activity as a consequence of the high polarization of the oligothienyl chain upon the replacement of the peripheral hydrogens by fluorine atoms). On the other hand, the B3LYP/6-31G** force field calculations also show that the outstanding IR absorption all of the oligomers display at 1650 cm^{-1}, which is missing in the FT-IR spectra of common oligothiophenes,[27] arises from a ν(C═C) stretching vibration located almost exclusively on the thienyl rings at both chain ends (see Figure 9). Its negligible chain-length frequency dispersion or constant peak position within the set of compounds is in agreement with its local mode character; however, its relative intensity does

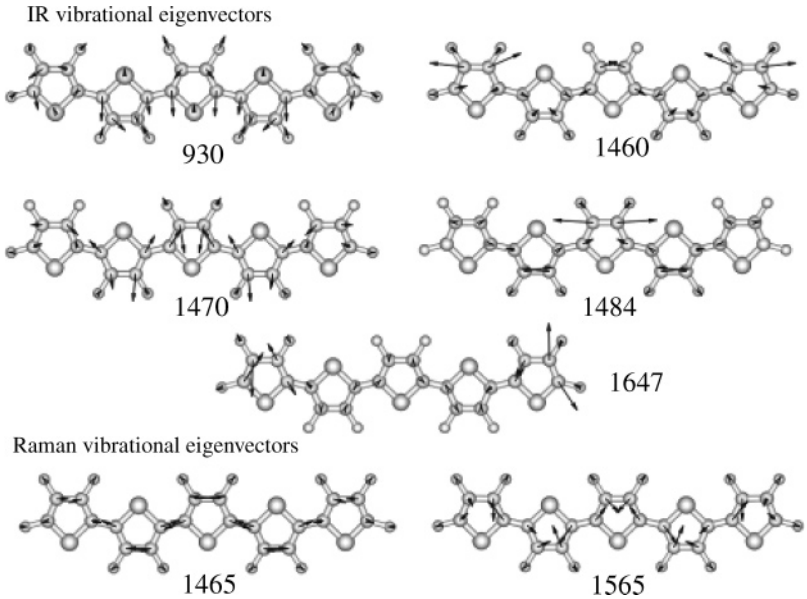

Figure 9. DFT//B3LYP/6-31G** vibrational eigenvectors associated with the most outstanding IR and Raman features of **PF-5T** (experimental IR/Raman frequency values are given in cm^{-1}).

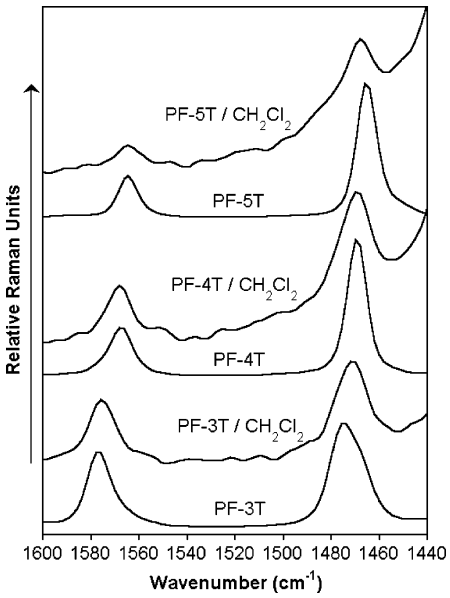

Figure 10. Comparison between the FT-Raman scattering profiles recorded for the three **PF-*n*T** oligomers as pure solids and as dilute solutes in CH_2Cl_2.

TABLE 4: Chain-Length Evolution of the Peak Positions of the Two Strongest Solid-State Raman Scatterings along the Whole Set of PF-*n*T Oligomers (Values Are Given in cm^{-1})

oligomer		
PF-3T	1577	1475
PF-4T	1567	1469
PF-5T	1565	1465

not vanish from the trimer to the pentamer (as should be the case for a chain-end vibration). This experimental observation must be related to the fact that the outside $C_\alpha{=}C_\beta$ bonds are much more polarized than the inner ones because they bear two fluorine substituents instead of only one.

Table 4 summarizes the evolution of the solid-state Raman peak frequencies upon chain-lengthening. By far, the two strongest Raman scatterings are those measured near 1470 and 1570 cm^{-1} (i.e., Figure 8 serves to illustrate their selective enhancement among the many Raman-active vibrations). The B3LYP/6-31G** vibrational eigenvectors depicted in Figure 9 show that the former is due to a totally symmetric ν_{sym}(C=C) stretching mode spreading over the whole π-conjugated backbone, along which all of the $C_\alpha{=}C_\beta$ bonds vibrate in-phase, whereas the latter arises also from a collective skeletal ν(CC) vibration of the oligothienyl spine, along which the whole sequence of thienyl $C_\beta{-}C_\beta$ and inter-ring $C_\alpha{-}C_{\alpha'}$ bonds shrink or lengthen in-phase. These two Raman-active skeletal vibrations are thus those mostly involved in the overall π-conjugation of these perfluorinated oligothiophenes. The downward dispersions of these two Raman scatterings from the trimer to the pentamer by 12 and 10 cm^{-1}, respectively, are nicely accounted for by DFT theory. However, theoretical wavenumbers are always lower than the experimental ones; this mismatch must be ascribed to the well-known tendency of B3LYP/6-31G** calculations to overestimate π-conjugation. Because dispersions toward lower frequencies of the ~1570 and 1470 cm^{-1} Raman scatterings with increasing number of units in the chain seemingly still do not reach saturation for **PF-5T**, it might occur that the "effective π-conjugation length" for these **PF-*n*T** oligothiophenes exceeds six or seven conjugated units.

We also observe that for the three oligomers, the peak positions and relative intensities of the ~1570 and 1470 cm^{-1} Raman scatterings are nearly the same (within 2−3 cm^{-1}) in the form of both a pure solid and as a dilute solute in CH_2Cl_2 (see Figure 10), thus indicating that (i) π-conjugation is the driving force that precludes for large conformational distortions in solution from the all-anti nearly coplanar arrangement of the solids, and (ii) crystal packing forces do not affect too much the π-conjugational properties of the individual molecules.

IV. Summary and Conclusions

This work presents an analysis of the molecular scale structural and electronic properties of a family of perfluorinated oligothiophenes, which could be ideally visualized as candidates for ambipolar transport in microelectronic devices. The analysis is done by means of a selection of spectroscopic tools (electron absorption and IR and Raman spectroscopies) whose data are carefully compared and combined with electrochemistry and supported by quantum chemical DFT calculations.

The Raman spectroscopic characterization of these molecular materials has been guided by DFT force field calculations and within the framework of the ECC theory that allows for the realization of the key Raman features mostly involved in the π-conjugation. Importantly, the collective characters of the ECC-related molecular vibrations and of the frontier molecular orbital wave functions (HOMO and LUMO) primarily determine the optical and electronic properties of this set of **PF-*n*T** oligomers. In this regard, the perfluorination of oligothiophenes promotes the stabilization of cathodic processes, which however still appear at higher electrochemical potentials than desired for their applicability in real devices. In detriment, the anodic features are shifted to higher energies. The chain-lengthening progressively mitigates the effect of perfluorination on the redox potentials, at the time that the effect of the overall π-conjugation upon interaction of an increasing number of neighboring thiophene rings becomes dominant for the largest members of the set of oligomers.

From a material science point of view, it is interesting to analyze the electrochemical band gap along a homologous set of molecular materials showing an amphoteric redox behavior because this magnitude (i.e., potential window that must be overcome for the injection of electrons and holes from an electrode) is directly related to the provided energy from a metallic junction of an electronic device (i.e., in field effect transistors) in which ambipolar transport of charge is required. It becomes clear that ambipolar transport in oligothiophenes can be attained through the attachment of electron-withdrawing groups to a central π-conjugated backbone and that the electrochemical band gap can be effectively tuned by controlling the molecular size.

Acknowledgment. Research at the University of Málaga was supported by the Ministerio de Educación y Ciencia (MEC) of Spain through project BQU2003-03194, and by the Junta de Andalucía for funding our FQM-0159 scientific group. M.C.R.D., R.P.O., and R.M.O. are also grateful to MEC and Junta de Andalucía for their personal doctoral grants.

References and Notes

(1) (a) Geiger, F.; Stoldt, M.; Schweizer, H.; Bäuerle, P.; Umbach, E. *Adv. Mater*. **1993**, *5*, 922. (b) Uchiyama, K.; Akimichi, H.; Hotta, S.; Noge, H.; Sakaki, H. *Mater. Res. Soc. Symp. Proc*. **1994**, *328*, 389.

(2) (a) Horowitz, G.; Fichou, D.; Peng, X.; Xu, Z.; Garnier, F. *Solid State Commun*. **1989**, *72*, 381. (b) Horowitz, G.; Peng, X.; Fichou, D.; Garnier, F. *J. Appl. Phys*. **1990**, *67*, 528. (c) Paloheimo, J.; Kuivalainen, P.; Stubb, H.; Vuorimaa, E.; Yli-Lahti, P. *Appl. Phys. Lett*. **1990**, *56*, 1157. (d) Akimichi, H.; Waragai, K.; Hotta, S.; Kano, H.; Sasaki, H. *Appl. Phys. Lett*. **1991**, *58*, 1500. (e) Waragai, K.; Akimichi, H.; Hotta, S.; Kano, H.;

Sasaki, H. *Synth. Met.* **1993**, *55*−*57*, 4053. (f) Garnier, F.; Hajlaoui, R.; Yassar, A.; Srivastava, P. *Science* **1994**, *265*, 1684. (g) Dodabalapur, A.; Katz, H. E.; Torsi, L.; Haddon, R. C. *Science* **1995**, *269*, 1560.

(3) Katz, H. E.; Torsi, L.; Dodabalapur, A. *Chem. Mater.* **1995**, *7*, 2235.

(4) Servet, B.; Horowitz, G.; Ries, S.; Lagorsse, O.; Alnot, P.; Yassar, A.; Deloffre, F.; Srivastava, P.; Hajlaoui, R.; Lang, P.; Garnier, F. *Chem. Mater.* **1994**, *6*, 1809.

(5) Horowitz, G.; Garnier, F.; Yassar, A.; Hajlaoui, R.; Kouki, F. *Adv. Mater.* **1996**, *8*, 52.

(6) Garnier, F.; Yassar, A.; Hajlaoui, R.; Horowitz, G.; Deloffre, F.; Servet, B.; Ries, S.; Alnot, P. *J. Am. Chem. Soc.* **1993**, *115*, 8716.

(7) Waragai, K.; Akimichi, H.; Hotta, S.; Kano, H.; Sakaki, H. *Phys. Rev. B* **1995**, *52*, 1786.

(8) Katz, H. E.; Dodabalapur, A.; Torsi, L.; Elder, D. *Chem. Mater.* **1995**, *7*, 2238.

(9) (a) Bao, Z.; Lovinger, A. J.; Brown, J. *J. Am. Chem. Soc.* **1998**, *120*, 207. (b) Katz, H. E.; Lovinger, A. J.; Johnson, J.; Kloc, C.; Siegrist, T.; Li, W.; Lin, Y. Y.; Dodabalapur, A. *Nature* **2000**, *404*, 478. (c) Facchetti, A.; Deng, Y.; Wang, A.; Koide, Y.; Sirringhaus, H.; Marks, T. J.; Friend, R. H. *Angew. Chem., Int. Ed.* **2000**, *39*, 4547.

(10) (a) Heidenhain, S. B.; Sakamoto, Y.; Suzuki, T.; Miura, A.; Fujikawa, H.; Mori, T.; Tokito, S.; Taga, Y. *J. Am. Chem. Soc.* **2000**, *122*, 10240. (b) Sakamoto, Y.; Suzuki, T.; Miura, A.; Fujikawa, H.; Tokito, S.; Taga, Y. *J. Am. Chem. Soc.* **2000**, *122*, 1832. (c) Sakamoto, Y.; Komatsu, S.; Suzuki, T. *J. Am. Chem. Soc.* **2001**, *123*, 4643.

(11) Frisch, M. J.; Trucks, G. W.; Schlegel, H. B.; Scuseria, G. E.; Robb, M. A.; Cheeseman, J. R.; Montgomery, J. A., Jr.; Vreven, T.; Kudin, K. N.; Burant, J. C.; Millam, J. M.; Iyengar, S. S.; Tomasi, J.; Barone, V.; Mennucci, B.; Cossi, M.; Scalmani, G.; Rega, N.; Petersson, G. A.; Nakatsuji, H.; Hada, M.; Ehara, M.; Toyota, K.; Fukuda, R.; Hasegawa, J.; Ishida, M.; Nakajima, T.; Honda, Y.; Kitao, O.; Nakai, H.; Klene, M.; Li, X.; Knox, J. E.; Hratchian, H. P.; Cross, J. B.; Adamo, C.; Jaramillo, J.; Gomperts, R.; Stratmann, R. E.; Yazyev, O.; Austin, A. J.; Cammi, R.; Pomelli, C.; Ochterski, J. W.; Ayala, P. Y.; Morokuma, K.; Voth, G. A.; Salvador, P.; Dannenberg, J. J.; Zakrzewski, V. G.; Dapprich, S.; Daniels, A. D.; Strain, M. C.; Farkas, O.; Malick, D. K.; Rabuck, A. D.; Raghavachari, K.; Foresman, J. B.; Ortiz, J. V.; Cui, Q.; Baboul, A. G.; Clifford, S.; Cioslowski, J.; Stefanov, B. B.; Liu, G.; Liashenko, A.; Piskorz, P.; Komaromi, I.; Martin, R. L.; Fox, D. J.; Keith, T.; Al-Laham, M. A.; Peng, C. Y.; Nanayakkara, A.; Challacombe, M.; Gill, P. M. W.; Johnson, B.; Chen, W.; Wong, M. W.; Gonzalez, C.; Pople, J. A. *Gaussian 03*, revision B.04; Gaussian, Inc.: Pittsburgh, PA, 2003.

(12) Becke, A. D. *J. Chem. Phys.* **1993**, *98*, 1372.

(13) Stephens, P. J.; Devlin, F. J.; Chabalowski, F. C. F.; Frisch, M. J. *J. Phys. Chem.* **1994**, *98*, 11623.

(14) Novoa, J. J.; Sosa, C. *J. Phys. Chem.* **1995**, *99*, 15837.

(15) Scott, A. P.; Radom, L. *J. Phys. Chem.* **1996**, *100*, 16502.

(16) Rauhut, G.; Pulay, P. *J. Phys. Chem.* **1995**, *99*, 3093.

(17) Francl, M. M.; Pietro, W. J.; Hehre, W. J.; Binkley, J. S.; Gordon, M. S.; Defrees, D. J.; Pople, J. A. *J. Chem. Phys.* **1982**, *77*, 3654.

(18) (a) Runge, E.; Gross, E. K. U. *Phys. Rev. Lett.* **1984**, *52*, 997. (b) Gross, E. K. U.; Ullrich, C. A.; Grossmann, U. J. In *Density Functional Theory*; Gross, E. K. U., Driezler, R. M., Eds.; Plenum Press: New York, 1995; p 149.

(19) Casida, M. E. In *Recent Advances in Density Functional Methods, Part I*; Chong, D. P., Ed.; World Scientific: Singapore, 1995; p 115.

(20) Koch, W.; Holthausen, M. C. *A Chemist's Guide to Density Functional Theory*; Wiley-VCH: Weinheim, 2000.

(21) Casado, J.; Miller, L. L.; Mann, K. R.; Pappenfus, T. M.; Kanemitsu, Y.; Ortí, E.; Viruela, P. M.; Pou-Amérigo, R.; Hernandez, V.; López Navarrete, J. T. *J. Phys. Chem. B* **2002**, *106*, 3872.

(22) Portmann, S.; Lüthi, H. P. *Chimia* **2000**, *54*, 766−770.

(23) Casado, J.; Ponce Ortiz, R.; Ruiz Delgado, M. C.; Azumi, R.; Oakley, R. T.; Hernandez, V.; Lopez Navarrete, J. T. *J. Phys. Chem. B* **2005**, *109*, 10115 and references therein.

(24) (a) Zhang, X.; Cote, A. P.; Matzger, A. J. *J. Am. Chem. Soc.* **2005**, *127*, 10502. (b) Mustafa, A. H.; Shepherd, M. K. *Chem. Commun.* **1998**, 2743. (c) Anthony, J. E.; Brooks, J. S.; Eaton, D. L.; Parkin, S. R. *J. Am. Chem. Soc.* **2001**, *123*, 9482.

(25) Sakamoto, A.; Furukawa, Y.; Tasumi, M. *J. Phys. Chem.* **1994**, *98*, 4635.

(26) (a) Yokonuma, N.; Furukawa, Y.; Tasumi, M.; Kuroda, M.; Nakayama, J. *Chem. Phys. Lett.* **1996**, *255*, 431. (b) Harada, I.; Furukawa, Y. In *Vibrational Spectra and Structure*; Durig, J., Ed.; Elsevier: Amsterdam, 1991; Vol. 19, p 369.

(27) (a) Hernandez, V.; Casado, J.; Ramirez, F. J.; Zotti, G.; Hotta, S.; Lopez Navarrete, J. T. *J. Chem. Phys.* **1996**, *104*, 9271. (b) Casado, J.; Hernandez, V.; Hotta, S.; Lopez Navarrete, J. T. *J. Chem. Phys.* **1998**, *109*, 10419. (c) Moreno Castro, C.; Ruiz Delgado, M. C.; Hernandez, V.; Hotta, S.; Casado, J.; Lopez Navarrete, J. T. *J. Chem. Phys.* **2002**, *116*, 10419. (d) Moreno Castro, C.; Ruiz Delgado, M. C.; Hernandez, V.; Shirota, Y.; Casado, J.; Lopez Navarrete, J. T. *J. Phys. Chem. B* **2002**, *106*, 7163. (e) Ruiz Delgado, M. C.; Hernandez, V.; Lopez Navarrete, J. T.; Tanaka, S.; Yamashita, Y. *J. Phys. Chem. B* **2004**, *108*, 2516. (f) Ruiz Delgado, M. C.; Casado, J.; Hernandez, V.; Lopez Navarrete, J. T.; Fuhrmann, G.; Bauerle, P. *J. Phys. Chem. B* **2004**, *108*, 3158. (g) Casado, J.; Ponce Ortiz, R.; Ruiz Delgado, M. C.; Azumi, R.; Oakley, R. T.; Hernandez, V.; Lopez Navarrete, J. T. *J. Phys. Chem. B* **2005**, *109*, 10115.

(28) (a) Casado, J.; Hernandez, V.; Hotta, S.; Lopez Navarrete, J. T. *J. Chem. Phys.* **1998**, *109*, 10419. (b) Casado, J.; Hernandez, V.; Hotta, S.; Lopez Navarrete, J. T. *Adv. Mater.* **1998**, *10*, 1258. (c) Casado, J.; Miller, L. L.; Mann, K. R.; Pappenfus, T. M.; Kanemitsu, Y.; Orti, E.; Viruela, P. M.; Pou-Amerigo, P.; Hernandez, V.; Lopez Navarrete, J. T. *J. Phys. Chem. B* **2002**, *106*, 3872. (d) Casado, J.; Miller, L. L.; Mann, K. R.; Pappenfus, T. M.; Hernandez, V.; Lopez Navarrete, J. T. *J. Phys. Chem. B* **2002**, *106*, 3597. (e) Casado, J.; Ruiz Delgado, M. C.; Shirota, Y.; Hernandez, V.; Lopez Navarrete, J. T. *J. Phys. Chem. B* **2003**, *107*, 2637. (f) Casado, J.; Hernandez, V.; Ponce Ortiz, R.; Ruiz Delgado, M. C.; Lopez Navarrete, J. T.; Fuhrmann, G.; Bauerle, P. *J. Raman Spectrosc.* **2004**, *35*, 592.

(29) (a) Hernandez, V.; Casado, J.; Effenberger, F.; Lopez Navarrete, J. T. *J. Chem. Phys.* **2000**, *112*, 5105. (b) Delgado Ledesma, S.; Ponce Ortiz, R.; Ruiz Delgado, M. C.; Vida, Y.; Perez-Inestrosa, E.; Casado, J.; Hernandez, V.; Kim, O.-K.; Lehn, J.-M.; Lopez Navarrete, J. T. *Chem.-Eur. J.* **2004**, *10*, 3805.

(30) (a) Gonzalez, M.; Segura, J. L.; Seoane, C.; Martin, N.; Garin, J.; Orduna, J.; Alcala, R.; Villacampa, B.; Hernandez, V.; Lopez Navarrete, J. T. *J. Org. Chem.* **2001**, *66*, 8872. (b) Casado, J.; Pappenfus, T. M.; Miller, L. L.; Mann, K. R.; Orti, E.; Viruela, P. M.; Pou-Amerigo, P.; Hernandez, V.; Lopez Navarrete, J. T. *J. Am. Chem. Soc.* **2003**, *125*, 2534.

(31) (a) Zerbi, G.; Castiglioni, C.; Del Zoppo, M. *Electronic Materials: The Oligomer Approach*; Wiley-VCH: Weinheim, 1998; p 345. (b) Castiglioni, C.; Gussoni, M.; Lopez Navarrete, J. T.; Zerbi, G. *Solid State Commun.* **1988**, *65*, 625. (c) Lopez Navarrete, J. T.; Zerbi, G. *J. Chem. Phys.* **1991**, *94*, 957 and 965. (d) Hernandez, V.; Castiglioni, C.; Del Zoppo, M.; Zerbi, G. *Phys. Rev. B* **1994**, *50*, 9815. (e) Agosti, E.; Rivola, M.; Hernandez, V.; Del Zoppo, M.; Zerbi, G. *Synth. Met.* **1999**, *100*, 101. (f) Zerbi, G. *Handbook of Conducting Polymers*; Marcel Dekker: New York, 1998.

(32) (a) Ehrendorfer, Ch.; Karpfen, A. *J. Phys. Chem.* **1994**, *98*, 7492. (b) Ehrendorfer, Ch.; Karpfen, A. *J. Phys. Chem.* **1995**, *99*, 5341.